Geotech Geol Eng (2013) 31:1107–1122
DOI 10.1007/s10706-013-9636-4

ORIGINAL PAPER

Small Strain Shear Modulus of Undisturbed Gravelly Soils During Undrained Cyclic Triaxial Tests

A. Flora · S. Lirer

Received: 19 October 2012 / Accepted: 11 March 2013 / Published online: 16 March 2013

Abstract The determination of the small strain shear modulus G_0 of gravels is a very important issue, both under monotonic or cyclic loading conditions. In the paper, the results of a series of triaxial tests carried out in a large apparatus on frozen (undisturbed) specimens of gravel are presented, along with the description of a new experimental device developed to measure the velocity of the shear waves V_s. During undrained cyclic tests, V_s values were measured before and after liquefaction, to analyse the effect of this peculiar stress history on the small strain stiffness G_0 of coarse grained soils. The small strain shear stiffness decreases as pore pressure in the specimen builds up. However, even in tests in which liquefaction was attained during the cyclic loading phase, G_0 showed to depend only on the current value of the effective stress: its values become smaller than the initial one (before cyclic loading was applied) but not nil, depending on the transient value of the pore pressure and therefore of the effective stress. Furthermore, the experimental results showed that, since there was no sudden drop of G_0 upon liquefaction triggering, the gravel did not have a structure which significantly affected its mechanical behaviour.

A. Flora · S. Lirer (✉)
Department of Hydraulic, Geotechnical and Environmental Engineering, University of Napoli Federico II, Naples, Italy
e-mail: stelirer@unina.it

Keywords Small strain shear stiffness · Shear wave velocity · Triaxial cell · Shear plates · Liquefaction

1 Introduction

Soil stiffness at very small strains, in the so called linear range, can be obtained with dynamic or static testing techniques. When using dynamic techniques, in which the velocity of the shear (S) waves (V_s) are recorded, the small strain shear stiffness (G_0) is calculated in the hypothesis of linear elasticity as:

$$G_0 = \rho \cdot V_S^2 \tag{1}$$

In which ρ is the density of the material through which the waves propagate. In laboratory, shear wave velocity measurements can be carried out during any kind of mechanical test, like triaxial tests (Sharma and Fahey 2004; Koseki et al. 1999; Zhou and Chen 2007), oedometer tests (Fam and Santamarina 1997), resonant column and torsional shear test (Santamatina and Cascante 1996; Youn et al. 2008) and in geotechnical centrifuge model (Lee et al. 2012). Most times, the measurement of V_s is confined to small size apparatuses, even though recently some applications to larger cells, necessary to test on coarse soils, have been recorded in literature (e.g. Modoni et al. 2000).

Among a wide variety of dynamic techniques, shear plates and bender elements are the most popular ones. The bender element technique (Shirley and Hampton 1978) is by far the most common method adopted in

laboratory apparatuses: an elastic shear wave is generated by a piezoceramic transducer placed on one end of the specimens (or on its side) and is received by another piezoceramic transducer placed at the other end (or on the opposite side). The shear wave velocity is calculated by measuring the travel time t (defined as the time required to cover the distance between the two transducers) and the distance between the two transducers. The determination of the waves travel time is still an open issue, due to the complexity of the wave's propagation process within the specimen and to the distortion of the wave during its travel. The signal interpretation technique affects the magnitude of the wave velocity and in turn the computation of the shear modulus G_0 (Mitatitonna et al. 2010).

Typically, soil shear stiffness is considered to depend on current stress state, void ratio and soil structure via a non linear equation. The stress state variable may be the mean effective stress invariant p' (Hardin and Black 1966) or a combination of the different principal effective stresses (e.g. Tatsuoka and Kohata 1994). In this paper, the previous formulation will be preferred, written as:

$$\frac{G_0}{p_a} = A \cdot f(e) \cdot \left(\frac{p'}{p_a}\right)^n \quad (2)$$

where p_a is a reference stress (usually taken equal to the atmospheric pressure) used for stress normalization, A is a non dimensional material constants accounting for soil nature (grading, mineralogy, fabric), n is an empirically determined exponent and f(e) is a function taking into account the effect of void ratio. In this work, the well known empirical equation proposed by Hardin and Richart (1963) has been adopted, which is:

$$f(e) = \frac{(2.17 - e)^2}{1 + e} \quad (3)$$

In the last decades, a huge amount of literature (e.g. Tatsuoka and Kohata 1994; Jang et al. 1997) has been dedicated to understanding the effect of intrinsic and state soil properties on small strain stiffness, and nowadays this is rather clear with no need to be replicated.

The shear modulus G_0 (or the shear wave velocity) at low strain levels is a very good index of the soil structure (e.g. Santamatina and Cascante 1996; Goto et al. 1999, Zhou and Chen 2007). Because of this, numerous studies have been conducted to get a correlation between shear wave velocity and liquefaction potential of natural deposits (Seed et al. 1983; Tokimatsu and Yoishida 1990; Yunmin et al. 2005).

Liquefaction is certainly a complex kind of stress–strain history, and the evolution of G_0 during a cycling load is certainly an issue. Goto et al. (1999), for instance, measuring small strain stiffness in triaxial liquefaction tests on Toyoura sand, observed a decrease of small strain stiffness during the test, which was more evident in the compression stages than in the extension ones. Santamarina and Aloufi (1999) analysed the influence of soil fabric changes on small strain stiffness by means of micro-mechanical experiments. They concluded that the relationship between the small strain stiffness and the stress history should capture the combined effect of contact behaviour, fabric changes, and the evolution of contact forces.

The large amount of laboratory experimental data available usually refers to clay and sand. Very few laboratory measurements of V_s were carried out on coarser soils, due to the need of larger testing apparatuses and to the larger energy needed for the artificially generated waveforms, difficult to obtain with bender elements. The available results on coarser soils (e.g. Koseki et al. 1999; Modoni et al. 2000; Hardin and Kalinski 2005) lead to conclusions similar to those obtained on sands and clays, even though the effect of the unavoidable non homogeneity within larger specimens may introduce a difference between static and dynamic measurements of G_0 (Modoni et al. 2000).

In this paper, experimental results obtained on undisturbed specimens of a coarse grained soil are reported, along with the description and the calibration of the experimental device developed to measure V_s in a large triaxial cell. Cyclic undrained stress paths were applied to quantify soil susceptibility to liquefaction. Shear wave velocities were measured before and after liquefaction, to try and see the effect of this peculiar stress history on the small strain stiffness of coarse grained soils.

2 Laboratory Test Equipment

2.1 Triaxial System and Wave Generating System

The experimental activity was carried out in a stress-path triaxial apparatus (Fig. 1) designed to accommodate large specimen (diameter $D_s = 200$ mm, height

$H_s = 400$ mm). It is well known that the reliability of laboratory tests largely depends on the ratio between D_s and the maximum particle size d_{max}. In the case of a coarse-grained soil, many authors (e.g. Marsal 1967) have suggested that the minimum limit value of this ratio is $D_s/d_{max} = 5$. Such a ratio, which is smaller than the one usually imposed in small triaxial apparatuses, has become widely adopted for coarse grained soils testing. In this work, since the specimens were frozen, grain size analyses were performed after testing. As will be shown in the next sections, however, in most cases there was no compatibility problem between the specimen size and the mean grain size.

The apparatus is controlled via a PC and is equipped with: two pressure transducers to measure cell and pore pressures, an internal load cell to measure the deviatoric stress, a volume gauge and two internal linear variable differential transformers (LVDTs) to measure the specimen' volumetric and axial strains. The apparatus has a maximum capacity of 800 kPa cell pressure. The triaxial (TX) cell is equipped with a special device conceived for dynamic measurements, following the idea originally put forward by Modoni et al. (2000): two electromagnetic actuators (one generates S wave and another P wave) and a three-dimensional accelerometer (see Fig. 2b, c) are placed on both the specimen pedestal and head (Fig. 2b). The actuator that generates S waves is made of a stainless still plate that enters into the specimen for about 15 mm. On demand, the plate is excited by an electromagnetic pulse (Fig. 2c). The actuator that generates P waves consists of a metal disk of about 20 mm of diameter, excited by a vertical electromagnet (Fig. 2c). Both actuators are included into a solid protection case and insulated from the mechanical structure of the pedestal and the head via a rubber glue layer. The effectiveness of this isolating detail, which is essential to avoid that waves travel through the very stiff steel frame of the triaxial cell, will be shown in § 2.3. The three-dimensional accelerometer, which is able to detect the arrival of both P and S waves, is located into a smaller cylindrical case and has a full scale range of 2 g in all three directions. The z axis of the accelerometer is vertically oriented; the x axis is oriented in the radial direction, and the y axis is oriented in the tangential direction. The accelerometers are insulated from the mechanical structure of the pedestal and head via a rubber glue layer.

The exact orientation of both the pedestal and the head is essential in setting up the test, to know the mutual

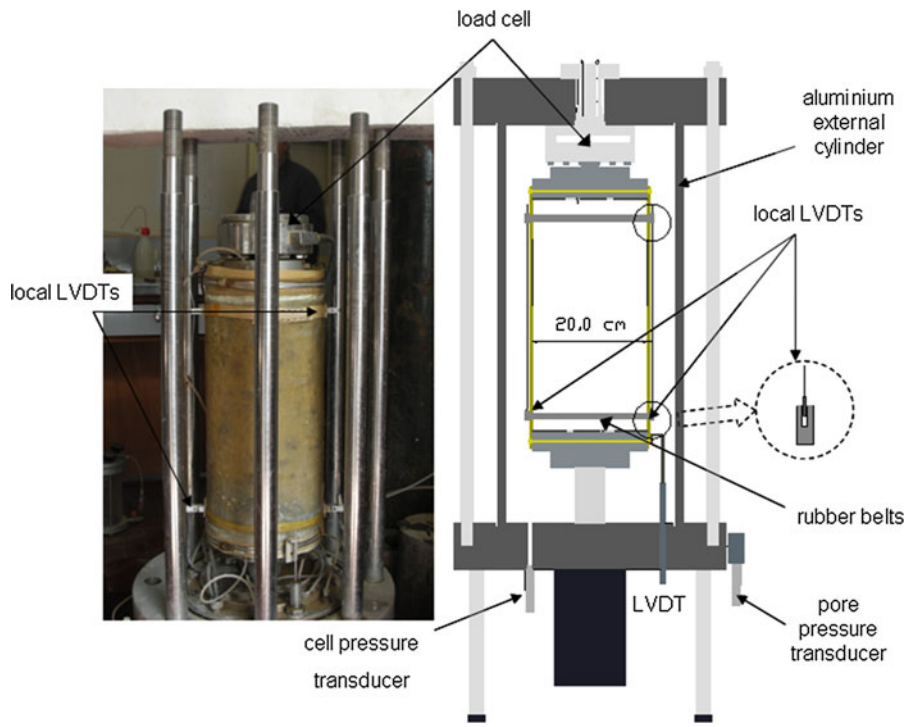

Fig. 1 Triaxial cell adopted in the experimental activity

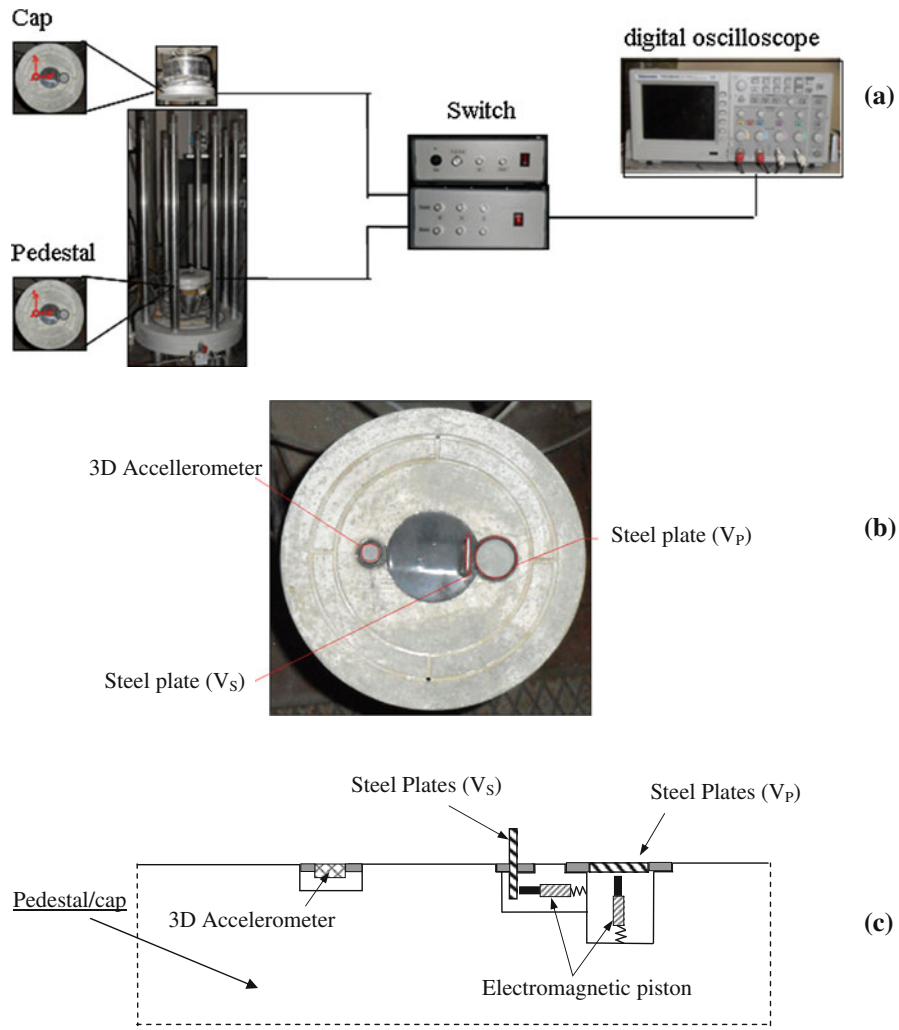

Fig. 2 System for dynamic measurements (**a**) and wave generating system (**b**, **c**)

orientation of the S waves generating and measuring devices. In any case, since most times gravels have an isotropic or at the most cross-anisotropic mechanical behaviour (i.e. the mechanical properties are identical in any horizontal direction), a possible misalignment of generator and actuator would not lead to any mistake, as long as the generated and measured signals are obtained by summing the two components in the x and y direction. In this work, perfect alignment was imposed and controlled on the results (one of the two components—the y one—being nil).

The four electromagnets (two on the pedestal and two on the head) are all independently driven by a pulse circuit. The two three-dimensional accelerometers (generating a total of six signals, three for each one), are powered and conditioned by a devoted electronics.

The input and output waveforms are automatically recorded by the digital oscilloscope (Fig. 2a). For the case of S waves, the out of polarization channels help to verify the correct working of the device. In principle, the starting time could be considered to coincide with the electric input to the electromagnetic generator. However, due to some possible mechanical delay of the hitting piston, such a measure could be affected by an error, thus leading to a misevaluation (overestimate) of the travel time. By assuming the starting time to coincide with the time at which the signal reaches the accelerometer close to the generator, such a mistake is avoided. In placing the specimen

in the cell, great care has to be taken to ensure a tight connection between it, the pedestal and the cap. When testing on frozen specimens, as it was done in this work, a hole was prepared on the two base and top faces of the specimens to insert the shear plates. After having prepared the holes (which had a rectangular section just slightly larger than shear plates cross section), they were filled with fine sand to guarantee the best possible contact between the plates and the specimen itself. Once the wave form (input and output wave forms) was registered on both specimen ends, the travel time was calculated as shown in the next section. Finally, wave velocities were calculated by knowing the current travel distance (continuously corrected because of the specimen's axial strain ε_a).

2.2 Definition of the Arrival Time

Many authors have commented the difficulty in identifying the exact time of arrival of the waves travelling into a specimen in laboratory (e.g. Viggiani and Atkinson 1995a; Arroyo et al. 2003; Mitatitonna et al. 2010) due to the complexity of the propagation process within the specimen. It is well known that compression (P) waves are faster than shear waves (S), and as a consequence they are the first ones to be detected at the arrival point.

Confining the discussion to shear waves, which are the ones that have been analyzed in this work, the most universal method adopted involves visually picking the arrival position from the received trace within the time domain record directly from an oscilloscope (Viggiani and Atkinson 1995). Several alternative technique, such as the cross-correlation method (Mancuso et al. 1989) or methods developed in the frequency domain, such as the phase delay method (Kaarsberg 1975; Greening and Nash 2004) have been proposed in literature.

In this study, the arrival time was computed based on the first rising point of the input and output waves, as shown for example in Fig. 3b. The figure shows the typical input and output S-wave signal: point A represents the moment of energy transfer from the source to the soil; and point B corresponds to the start of receiver motion.

2.3 Calibration of the Experimental Device for Calculating V_s

Since the dynamic system inserted into the large triaxial cell is a prototype, a calibration was needed to

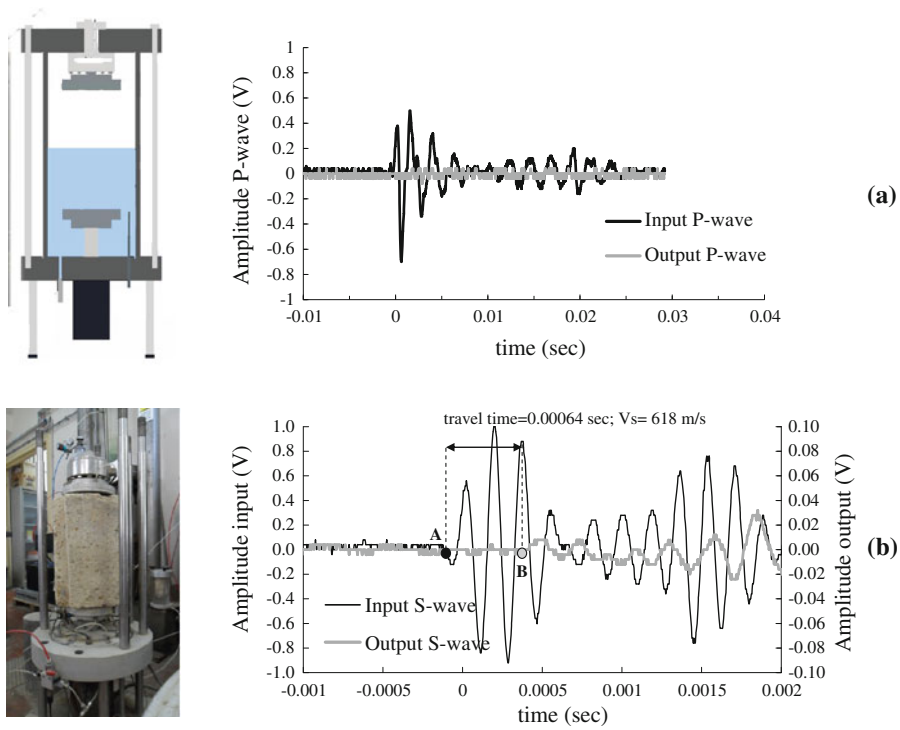

Fig. 3 Examples of check tests for the calibration of the experimental device to calculate the travel time of waves: **a** triaxial apparatus partially filled with distiller water, input and output P waves; **b** test on soft rock specimen, showing input and output S waves, used to calculate V_s

be sure that the generated waves travel within the specimen and not through the cell stiff steel structure (base, confining cylinder, rods, top cap). Many tests were carried out to this aim. For the sake of brevity, two examples of the different check tests carried out are reported in Fig. 3: the first kind of test (Fig. 3a) was carried out without specimen, just partially filling the cell with water (with different filling percentages), and generating both S and P waves. Such a kind of test was carried out to verify that the isolation of the wave generators from the cell was effective, and therefore the very stiff cell frame did not transmit the waves from one base to the other: since there is no solid continuity within the cell, neither P waves nor S waves should be recorded at the receiver. As the figure shows (for P-wave), no signal was recorded in all tests. This was a confirmation that the rubber isolation of the generating and measuring systems was well conceived. Eventually, when the cell was completely filled with water, only compression waves were recorded at the other end of the cell, with the typical velocity they have when travelling in water, while no S wave could be detected. In the other type of tests (Fig. 3b), S waves were generated and propagated through a soft rock specimen (in this case, Neapolitan Yellow Tuff) whose typical values of V_s were well known. The goal of this kind of tests was to verify that the contact between the shear plates and the specimen was well conceived, being the soft rock in all similar to the frozen specimen to be tested. Since during these check tests the recorded values of V_s were similar to those typical for this soft rock (Vinale 1988), it was demonstrated that specimen preparation and placing in the cell was correctly carried out, and the fine sand put within the hole prepared to insert into the specimen the shear plates ensured a close contact.

3 Experimental Activity

3.1 Test Materials

The experimental activity was carried out on specimens obtained from frozen samples recovered in Calabria (Southern Italy), at Cannitello site, near the well known Messina Strait that separates Sicily from Italy mainland. The frozen samples where retrieved at depths ranging between 18 and 33 m from the ground surface, in a normally consolidated coarse-grained Holocene soils deposit (locally known as *Coastal Deposits*). The in situ freezing technique and specimen preparation are described in Flora et al. 2012 and Fioravante et al. 2012 (these latter authors working on coarse grained soils retrieved close to the Messina Strait but on the Sicilian side). For cohesionless soils, soil freezing is the only technique available to try and limit the damage during coring under ground water level. Comparing shear wave velocities measured in situ in Cross Hole tests and in laboratory during triaxial testing, Fioravante et al. (2012) have found that they assume similar values, thus showing that the retrieved samples are undisturbed. A similar comparison will be shown in the following for the materials used in this work.

After testing, soil gradings were obtained for all the specimens (Fig. 4). In our case, they can be divided into three different families: a uniform sand with a very low percentage of gravel (soil A), a gap graded coarser soil with a sandy matrix and large particles (soil B), and an even coarser well-graded sandy gravel (soil C). The mean relevant physical and mechanical properties of the three soil families are summarized in Table 1.

A large experimental activity was developed to analyse the behaviour of all these soils under monotonic and cyclic triaxial stress paths (Flora et al. 2012). In the monotonic tests, the typical behaviour of coarse-grained soils was always observed, with very little or no peak in shear strength, along with a dilative behaviour. Furthermore, the uniform sand A and the gap-graded gravelly sand B, differing only in a small amount of the coarser fraction, exhibit a similar

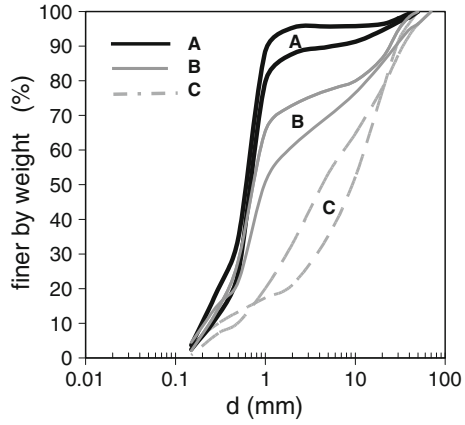

Fig. 4 Ranges of grain size distributions of the tested specimens

Table 1 Physical and mechanical properties of the tested soils (Flora et al. 2012)

Soil	d_{max} (mm)	d_{50} (mm)	C_u (D_{60}/D_{10})	G_s	φ_u* (°)
A	50	0.7	2.8	2.70	38.6
B	50	1.0	6.6		39.6
C	70	10.0	26		43.2

* Ultimate friction angle (at axial strain $\varepsilon_a = 20$ %) from monotonic tests

mechanical behaviour under both monotonic and cyclic loading and in the following they will be therefore analyzed together.

3.2 Specimens Preparation and Testing Programme

The testing programme (Table 2) consists in a series of undrained cyclic triaxial tests: eight of them have been carried out on frozen specimens and only one on a reconstituted specimen.

The thawing of the frozen specimens took about 24 h, and was carried out imposing a low isotropic effective stress ($\sigma'_c = 20$ kPa) in drained conditions, with a back pressure of 30 kPa. Consistently with the indications of Tanaka et al. (1991), in all cases it was experimentally observed that the effects of membrane penetration during thawing were negligible. Upon thawing, specimen saturation (Skempton parameter $B \geq 98$ %) was guaranteed by water flow under a very low hydraulic gradient.

The reconstituted specimen (C10r in Table 2) has been prepared by wet tamping at the same void ratio of the undisturbed specimens from which the material was retrieved (C10 in Table 2). A small unavoidable difference in void ratio resulted.

Both isotropic (CCIU tests in Table 2) and anisotropic consolidation stress paths (CCK_0U tests in Table 2) were adopted prior to the cyclic shearing stage, with the latter used to simulate in situ K_0 initial stress state. Being very difficult the computation of the coefficient of earth pressure at rest K_0 of gravelly soils from laboratory tests (Lirer et al. 2011), in this study K_0 was obtained from in situ measurements($K_0 = 0.47$, Fiammenghi et al. 2009). In all cyclic tests, the axial loading was applied through uniform sinusoidal cycles with constant amplitude at a frequency of 0.1 Hz.

In undrained cyclic triaxial tests, the imposed cyclic stress ratio CSR is defined as the ratio between the shear stress τ_d and the normal effective stress σ'_{ref} acting on a plane inclined at 45° on the horizontal plane (i.e. on the plane of maximum shear stress):

$$CSR = \frac{\tau_d}{\sigma'_{ref}} = \frac{q_d}{2\sigma'_{ref}} \quad (4)$$

where q_d is the cyclic deviatoric stress. By definition, σ'_{ref} is equal to:

$$\sigma'_{ref} = \frac{\sigma'_{1,c} + \sigma'_{3,c}}{2} \quad (5)$$

where $\sigma'_{1,c}$ and $\sigma'_{3,c}$ are respectively the maximum and the minimum principal effective stresses acting on

Table 2 Experimental programme

Soil	Name	Stress path	e_0	ρ (kg/m^3)	$\sigma'_{3,c}$ (kPa)	$\sigma'_{1,c}$ (kPa)	$V_{S,0}$ (m/s)	CSR	N_{cyc} Liquef. ($R_u = 0.9$)	N_{cyc} Liquef. ($\varepsilon_{DA} = 5$ %)
A,B	C10	CCIU	0.600	1962	200	200	567	0.240	85	–
	C10r**	CCIU	0.530	1980	200	200	548	0.240	82	–
	C5	CCIU	0.570	2066	200	200	606	0.220	29	–
	C6	CCK_0U	0.370	2254	94	200	560	0.580	–	7
	C8	CCK_0U	0.700	1970	94	200	530	0.330	c.m.*	
	C12	CCK_0U	0.580	2025	94	200	533	0.430	c.m.*	
C	C-C6	CCIU	0.483	2079	400	400	559	0.350	6	–
	C-C10	CCIU	0.462	2110	200	200	550	0.320	7	–
	C-C8	CCK_0U	0.524	1790	94	200	632	0.500	11	22

* Cyclic mobility

** Test on reconstituted specimens

the specimen at the end of the consolidation phase. In isotropically consolidated tests ($\sigma'_{1,c} = \sigma'_{3,c}$), σ'_{ref} is equal to the consolidation pressure.

The cyclic resistance ratio CRR is defined as the value of CSR causing soil liquefaction in a given number of loading cycles.

It is well known that loose saturated cohesionless soils, during cyclic undrained tests can either undergo liquefaction or cyclic mobility, depending on the applied consolidation and cyclic stress path (Robertson 1994). In fact, during cyclic undrained loads such soils develop positive pore pressures due to their contractive behaviour: if the effective stress state can progress to the point of zero effective stress, liquefaction is attained. On the contrary, if during cyclic undrained loads soil undergoes cumulative permanent axial strain but the stress path remains stable after many cycles without transient states of zero effective stress, cyclic mobility takes place.

In cyclic triaxial tests it is usually assumed that liquefaction is attained when a conventional stress or strain thresholds is reached. The stress-based approach typically refers to the pore pressure ratio R_u, defined as the ratio between the cyclically induced pore pressure increment Δu and the confining stress σ'_c ($R_u = \Delta u/\sigma'_c$). The strain-based approach (which may be alternatively used when R_u does not reach the critical value but large strains take place) typically assumes a limit value for the double amplitude axial strain ε_{DA}. In this work liquefaction was identified by means of a stress threshold ($R_{u,liq} = 0.9$) or a strain threshold ($\varepsilon_{DA,liq} = 5.0$ %).

It must be stressed out, however, that V_s measurements (and consequently G_0 calculations via Eq. 1) are carried out instantaneously, thus at some precise values of the current stress state (synthetically represented by q and R_u). Therefore, even after liquefaction is seen to take place, the current values of R_u (or ε_{DA}) could be smaller than the assumed threshold, depending on the time at which the wave generator is activated. As a consequence, even after liquefaction starts the transient effective stress state could be large enough to be comparable with the ones experienced by the specimen before liquefaction. Then, the comparison between V_s values at a given stress state before and after liquefaction, when any trace of the structure has been swept off by the very large cyclic strains, may be taken as a measure of the relevance of soil structure on soil behaviour: in fact, similar results would indicated that, for the tested soil, the structure has little effect on the stress–strain behaviour of the soil, and only traditional state variables play a role (density and stress state, or for instance the more synthetic state parameter ψ proposed by Been et al. 1991). On the contrary, large differences would indicate that the original structure, affects soil behaviour, and therefore plays a relevant role.

4 Experimental Results

Cannitello site was extensively investigated with in situ tests prior to freezing and coring. In particular, crosshole tests (CH) were carried out to get the V_S profile with depth. An example taken from the paper by Fiammenghi et al. (2009) is reported in Fig. 5. In the figure, soil grading, penetration resistance to SPT and LPT (Large Penetration Test, see Fiammenghi et al. 2009), energetic efficiency ER of the penetration tests and shear wave velocity profiles with depth are reported. On the V_S profile, the range of depths at which the frozen specimens were retrieved is evidenced (18 m $< z <$33 m). At these depths, the values of V_S measured in situ range from a minimum of about 370 m/s to a maximum of 600 m/s (not considering a single very high value of 750 m/s).

Such results will be compared with the ones obtained in laboratory to check specimen's quality: if the specimens are really undisturbed, V_S values measured in laboratory should be comparable with the ones obtained in situ via CH tests.

4.1 Shear Wave Velocity Measurements

4.1.1 Soil A/B

In all cases, the value of Vs after consolidation ($V_{s,0}$) has been measured (see Table 2): such values are in good accordance with the ones obtained via the in situ CH tests (Fig. 5), in which V_S varies from 532 to 604 m/s. The results of the cyclic undrained tests carried out on specimens of soils A and B (Table 2) are plotted in four different planes from Figs. 6 to 10. Two tests (C10 and C5) were performed on isotropically consolidated specimens (CCIU) and three tests (C6, C8 and C12) on anisotropically consolidated specimens (CCK_0U). In CCIU tests C10 and C5 (Figs. 6 and 7) both specimens liquefied, reaching the stress

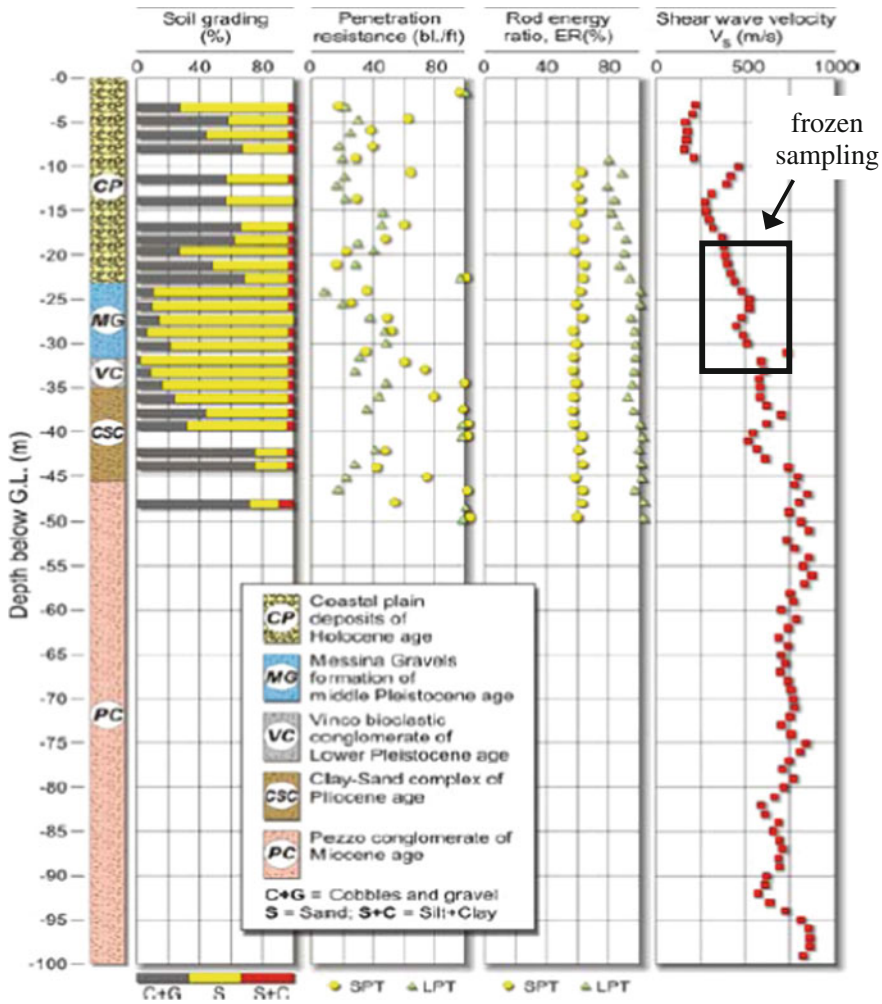

Fig. 5 Soil profile at Calabria tower site (after Fiammenghi et al. 2009)

thresholds $R_{u,liq} = 0.9$ respectively after a number of cycles $N_{cyc,C10} = 85$ and $N_{cyc,C5} = 29$. In the figures, the shear wave velocity V_s measured during these two cyclic tests is plotted versus the corresponding pore pressure ratio R_u. The measured values of Vs keep a fairly constant value up to $R_u \approx 0.4$, to get slightly smaller values for larger values of R_u. In these two tests, however, the dynamic Vs measurements have been carried out only prior to liquefaction, and as a consequence only before a possible dramatic change of soil structure.

Figure 8 shows the results of the CCK_0U test named C6, carried out on an anisotropically consolidated specimen (Table 2): in this case liquefaction is considered to occur after 7 cycles, when the double amplitude axial strain in each cycle (ε_{DA}) reaches the assumed strain threshold ($\varepsilon_{DA,liq} = 5.0$ %). The maximum value of the cyclic pore pressure ratio ($R_{u,max} \approx 0.4$) reached after 12 cycles is significantly lower than $R_{u,liq}$. In this case, some Vs measurements have been carried out after the strain threshold was attained, therefore during liquefaction. In the figure, the measurements carried out after liquefaction are represented by black dots. It can be noted that Vs seems to depend on R_u only, and no visible difference can be seen before and after liquefaction. This indicates that structure does not play a relevant role in the mechanical behaviour of this specimen. Even after liquefaction, the values of V_s have been calculated only at values of R_u not particularly large ($R_{u,max} \approx 0.4$). By comparing these results with the ones of the other two tests previously shown (Figs. 6 and 7), a larger decrease of V_s with R_u can be observed.

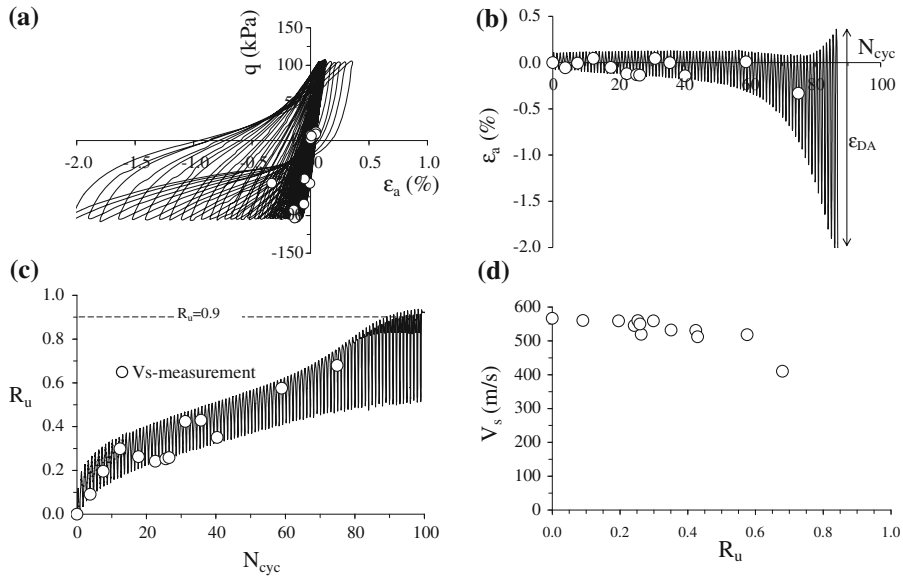

Fig. 6 Results of the CCIU test C10 (Table 2): **a** deviatoric stress q versus axial strain ε_a; **b** axial strain ε_a versus number of cycles N_{cyc}; **c** cyclic pore pressure ratio R_u versus number of cycles N_{cyc}; **d** shear wave velocity V_s versus cyclic pore pressure ratio R_u

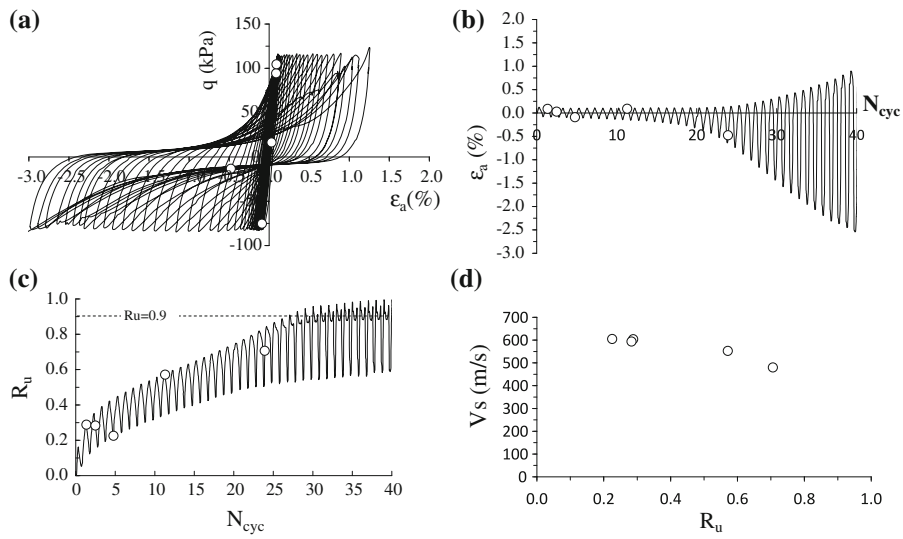

Fig. 7 Results of the CCIU test C5 (Table 2): **a** deviatoric stress q versus axial strain ε_a; **b** axial strain ε_a versus number of cycles N_{cyc}; **c** cyclic pore pressure ratio R_u versus number of cycles N_{cyc}; **d** shear wave velocity V_s versus cyclic pore pressure ratio R_u

In CCK_0U tests C8 and C12 (Figs. 9 and 10), the last two carried out on the group of specimens of soils A and B, no liquefaction occurred, and the soil underwent cyclic mobility. The specimens show cumulative permanent axial strain in the compression plane, but the double amplitude axial strain in each cycle remains always very small ($\varepsilon_{DA} \lll \varepsilon_{DA,liq}$). At the same time, the cyclically induced pore pressure increments keep very low values ($R_{u,max} = 0.25$ in tests C8, $R_{u,max} = 0.45$ in tests C12) even after a large number of cycles. For these two tests, the measured shear wave velocities don't change significantly during the tests.

4.1.2 Soil C

In all cases, the value of V_S after consolidation ($V_{S,0}$) has been measured (see Table 2): again, such values are in good accordance with the ones obtained via the in situ CH tests (Fig. 5). The results of the three cyclic tests carried out on specimens of soil C (Table 2) are plotted from Figs. 11 to 13. Two tests (C-C6 and

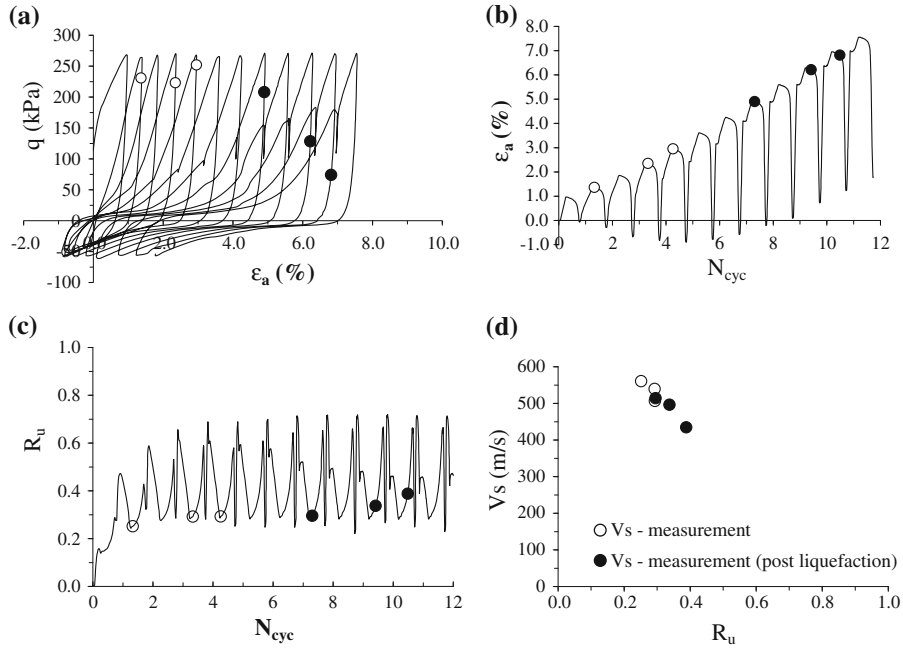

Fig. 8 Results of the CCK_0U test C6 (Table 2): **a** deviatoric stress q versus axial strain ε_a; **b** axial strain ε_a versus number of cycles N_{cyc}; **c** cyclic pore pressure ratio R_u versus number of cycles N_{cyc}; **d** shear wave velocity V_s versus cyclic pore pressure ratio R_u

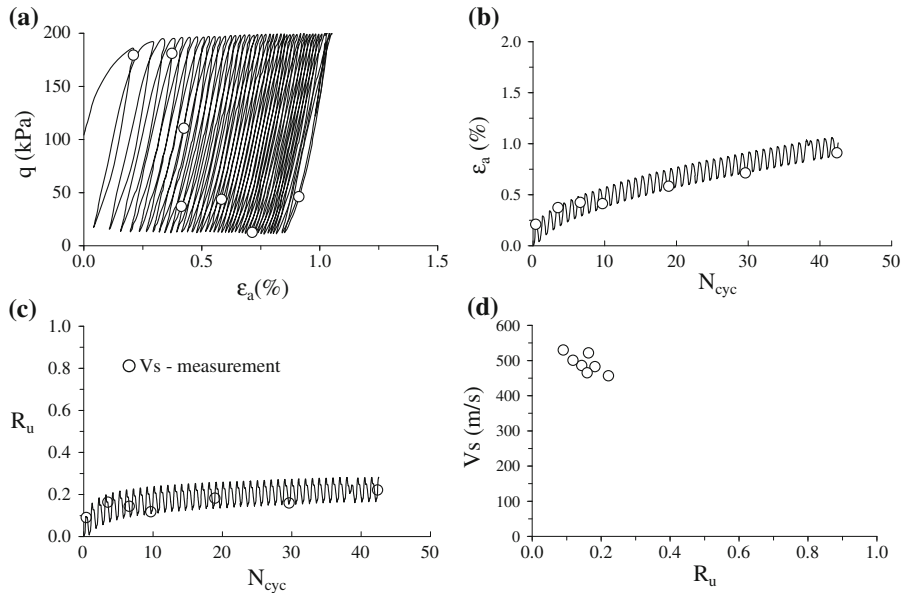

Fig. 9 Results of the CCK_0U test C8 (Table 2): **a** deviatoric stress q versus axial strain ε_a; **b** axial strain ε_a versus number of cycles N_{cyc}; **c** cyclic pore pressure ratio R_u versus number of cycles N_{cyc}; **d** shear wave velocity V_s versus cyclic pore pressure ratio R_u

C-C10) have been performed on isotropically consolidated specimens (CCIU) and only one (C-C8) on anisotropically consolidated specimens (CCK_0U). For both the CCIU tests, liquefaction was attained ($R_u > R_{u,liq}$) after few cycles ($N_{cyc,C6} = 6$ and $N_{cyc,C10} = 7$). Shear wave velocity V_s keeps in these two tests a rather constant value, with only a slight decrease with R_u. Again, after liquefaction (black dot, Fig. 12), the value of V_s does not show any sudden drop, and keeps aligned with the ones previously measured, thus confirming that in this case structure does not play any significant role on the small strain mechanical behaviour of the soil. Consistently with these results, also for the CCK_0U test C-C8 (Fig. 13), for which liquefaction was attained after 11 cycles ($R_u > R_{u,liq}$), V_S values keep a rather constant value

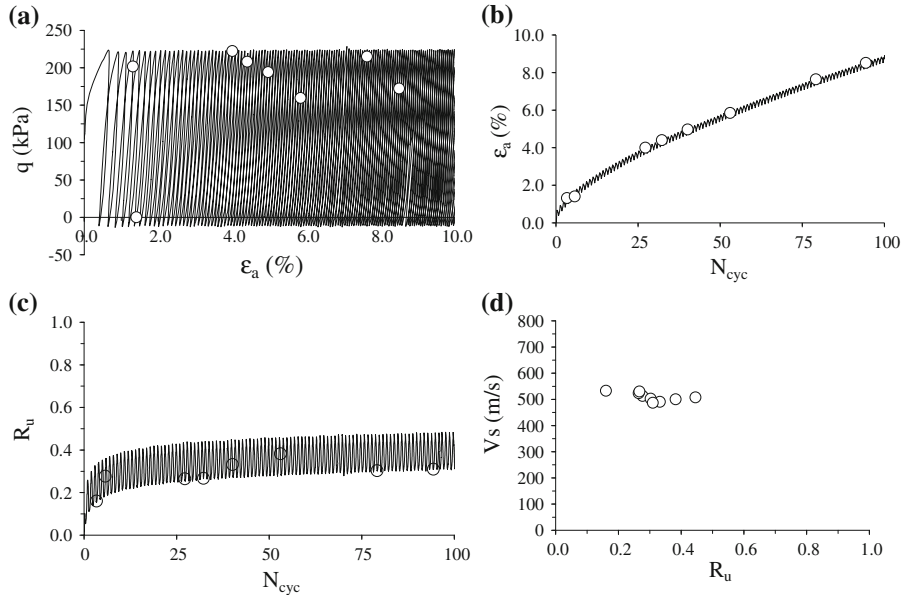

Fig. 10 Results of the CCK_0U test C12 (Table 2): **a** deviatoric stress q versus axial strain ε_a; **b** axial strain ε_a versus number of cycles N_{cyc}; **c** cyclic pore pressure ratio R_u versus number of cycles N_{cyc}; **d** shear wave velocity V_s versus cyclic pore pressure ratio R_u

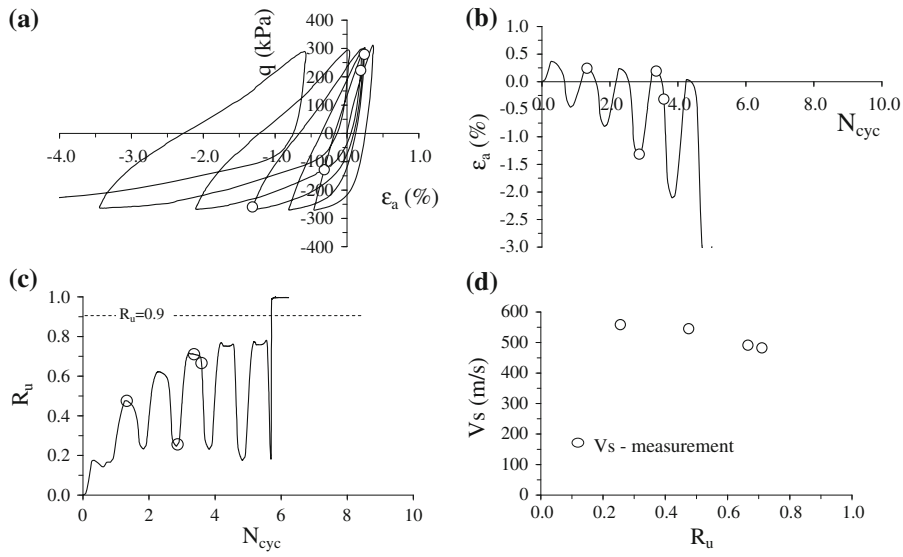

Fig. 11 Results of the CCK_0U test C-C6 (Table 2): **a** deviatoric stress q versus axial strain ε_a; **b** axial strain ε_a versus number of cycles N_{cyc}; **c** cyclic pore pressure ratio R_u versus number of cycles N_{cyc}; **d** shear wave velocity V_s versus cyclic pore pressure ratio R_u

up to $R_u \approx 0.4$, showing a slight decrease for larger values of R_u.

4.2 Shear Modulus G_0

The V_S measurements of all the tests were processed to calculate the shear modulus G_0 via Eq. 1. The values of $G_{0,max}$ (G_0 after consolidation phase) obtained in all the tests (reported in Fig. 14a, b) are similar to the ones obtained by Modoni et al. (2000) for a similar gravelly soil (Nacaome gravel) in a large triaxial apparatus equipped for the dynamic measurements with a device similar to the one adopted in this research.

In order to exclude the influence of the variation in void ratio (e) among the tested specimens (Table 2), the values of G_0 obtained from dynamic measurements were also normalized by using the function f(e) given in Eq. (3). All the experimental results have then been summarized in Fig. 14. In particular, being $G_{0,max}$ the

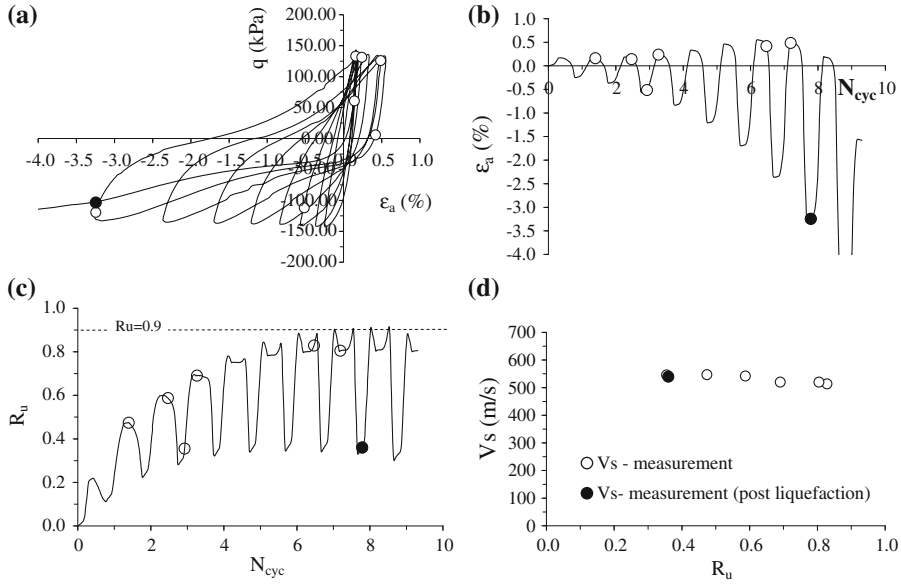

Fig. 12 Results of the CCK_0U test C-C10 (Table 2): **a** deviatoric stress q versus axial strain ε_a; **b** axial strain ε_a versus number of cycles N_{cyc}; **c** cyclic pore pressure ratio R_u versus number of cycles N_{cyc}; **d** shear wave velocity V_s versus cyclic pore pressure ratio R_u

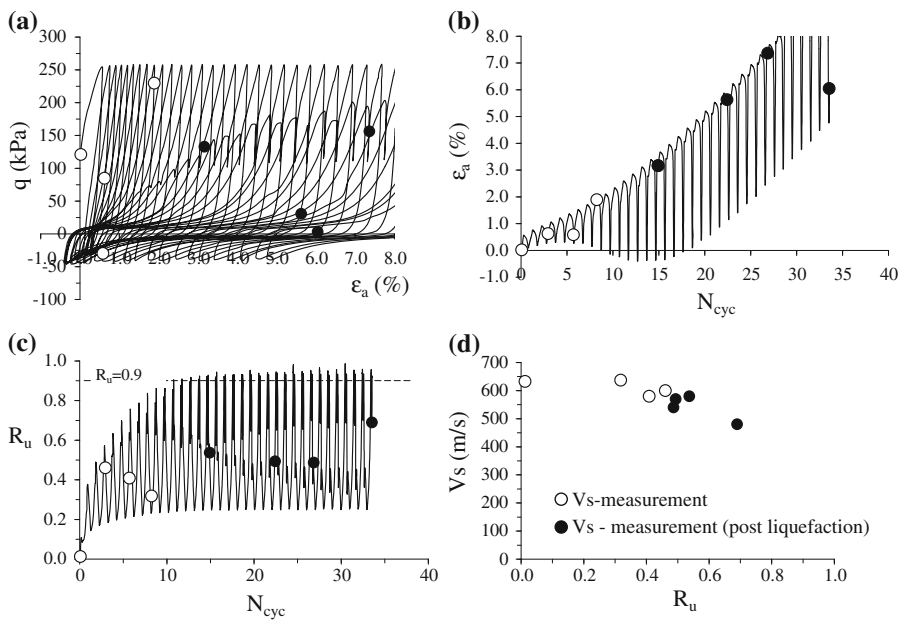

Fig. 13 Results of the CCK_0U test C-C8 (Table 2): **a** deviatoric stress q versus axial strain ε_a; **b** axial strain ε_a versus number of cycles N_{cyc}; **c** cyclic pore pressure ratio R_u versus number of cycles N_{cyc}; **d** shear wave velocity V_s versus cyclic pore pressure ratio R_u

value of G_0 calculated after consolidation, the results have been first plotted in a $G_0/G_{0,max}$ versus R_u plane, putting all the results together for each soil (A/B in Fig. 14a, c in Fig. 14b). The two plots seem to indicate that, even though $G_{0,max}$ is similar in the two soils, the dependence of the small strain shear stiffness on R_u is different, being soil C stiffer than soil A/B. This is consistent with some indications in literature (e.g. Modoni et al. 2000) and with the larger shear strength observed for soil C (Flora et al. 2012).

Finally, the comparison (Fig. 14a) between the results of test C10 (frozen specimen) and C10r (reconstituted specimen) indicate that the structure of the soil has no major effect on its mechanical behaviour, as both the normalized decay curves and the values of $G_{0,max}$ are similar.

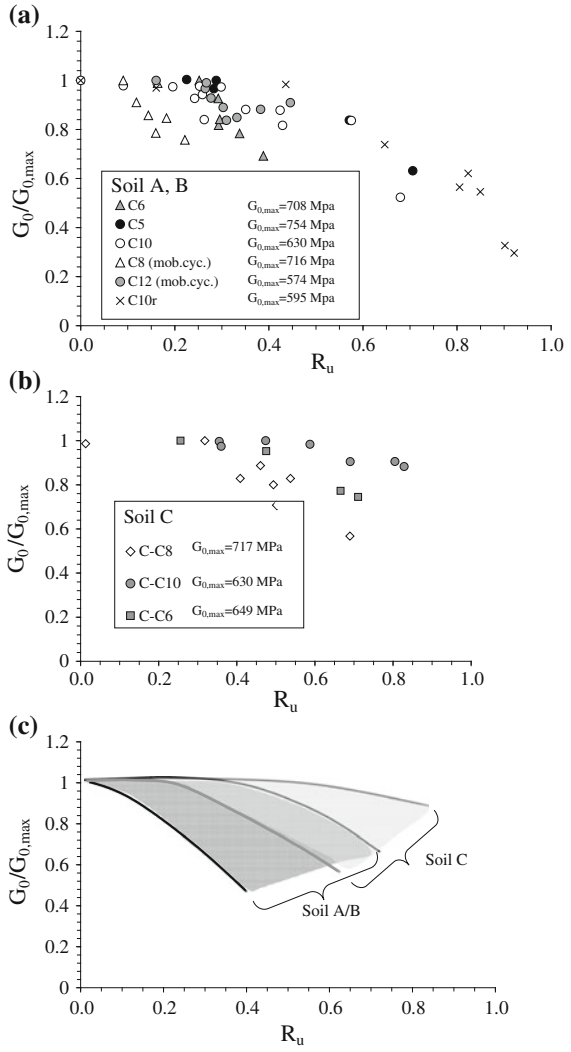

Fig. 14 Normalized small strain shear modulus $G_0/G_{0,max}$ versus the pore pressure ratio R_u, **a** results of tests on soil A/B, **b** results of tests on soil C

Figure 14c summarizes this experimental observation in a qualitative plot, in which the two different ranges of values are indicated.

Finally, the results are plotted in Figs. 15a, b in a $G_0/f(e)p_a$ versus p'/p_a plane, along with the best fitting curve obtained via Eq. 2. Consistently with the experimental observations previously reported, the exponent of the best fitting curve for soil C is smaller. The figure shows that Eq. (2), which assumes that G_0 is related to the mean effective stress p' and not to the single effective stress components, is well suited to this case, as the data are nicely correlated to p'/p_a.

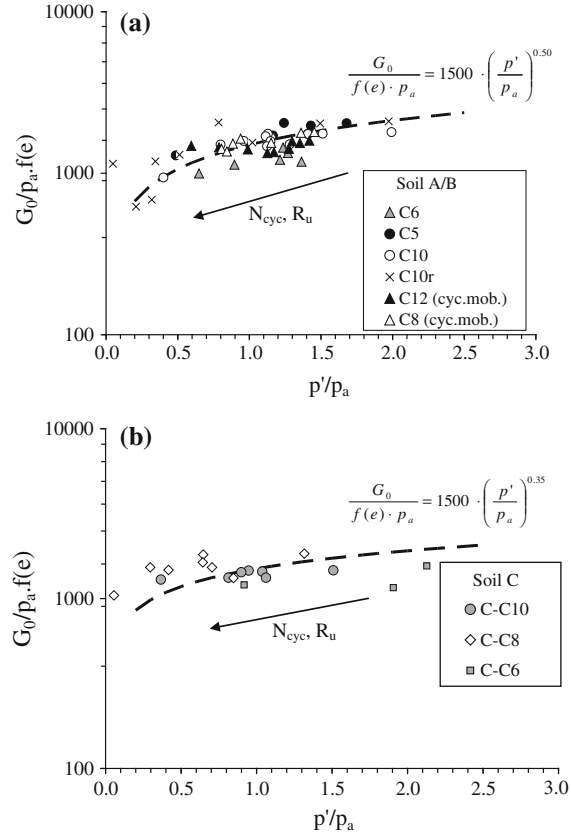

Fig. 15 Normalized small strain shear modulus of soil A/B (**a**) and soil C (**b**) versus the normalized mean effective stress (p' is the mean effective stress invariant and p_a the atmospheric pressure)

5 Conclusion

The measurement of V_S in coarse grained soils before and after cyclic loads is a very important issue. This paper presents the results obtained on undisturbed specimens of coarse grained soils, tested in a large triaxial cell equipped with prototype shear plates. The system adopted to generate and measure waves travelling within the specimen has been calibrated and proved to be effective. The $V_{S,0}$ (after the consolidation phase) values measured in laboratory are comparable with the ones obtained in situ via CH tests.

The results obtained from the undrained cyclic triaxial tests on the undisturbed specimens have shown that, for the tested coarse grained soils, V_S and G_0 values do not show a dramatic decrease with pore pressure build up (synthetically represented by R_u).

Furthermore, V_S (or G_0) values obtained after liquefaction has been triggered do not show a trend different from the one of the values obtained before.

This result, which has been obtained on undisturbed specimens, indicates that in this case the structure of the soil has no effect on its mechanical behaviour.

Acknowledgments The authors gratefully acknowledge thank dot. Fiammenghi of *Stretto di Messina S.p.A.* for allowing the publication of the experimental results.

References

Arroyo M, Muir WoodD, Greening PD (2003) Source near-field effects and pulse tests in soil samples. Gèotecnique 53(3):337–345

Been K, Jefferies M, Hachey J (1991) The critical state of sands. Geotechnique 41(3):365–381

Fam M, Santamarina JC (1997) A study of consolidation using mechanical and electromagnetic waves. Géotechnique 47(2):203–219

Fiammenghi G, Jamiolkowski M, Van Impe F (2009) Geotechnical engineering issues related to the Messina Strait Crossing. 5th international symposium on deep foundations on Bored and Auger Piles (BAP V), 8–10 September 2008, Ghent, Belgium, Edited by W.F. Van Impe and P. O, 3–19

Fioravante V, Giretti D, Jamiolkowski M, Rocchi G (2012) Triaxial tests on undisturbed gravelly soils from the sicilian shore of the messina strait. Bull Earthq Eng 10(6): 1717–1744

Flora A, Lirer S, Silvestri F (2012) Undrained cyclic resistance of undisturbed gravelly soils. Soil Dyn Earthwake Eng 43:366–379

Goto S, Matsueda S, Morii Y, Sueoka T (1999) Small strain stiffness of sands in isotropic compression and liquefaction tests. Proceedings of the 2th International Symposium on Pre-Failure deformation characteristic of geomaterials. IS Torino, 1: 275–281

Greening PD, Nash DFT (2004) Frequency domain determination of go using bender elements. Geotech Test J 27(3):288–294

Hardin BO, Black WL (1966) Sand stiffness under various triaxial stresses. J Soil Mech Found Div, ASCE 92(SM2): 27–42

Hardin BO, Kalinski ME (2005) Estimating the shear modulus of gravelly soils. J Geotech Geoenviron Eng, ASCE 2005:867–875

Hardin BO, Richart FE (1963) Elastic wave velocities in granular sands. J Soil Mech Found Div, ASCE 89(SM1):33–65

Jang GL, Tatsuoka F, Flora A, Koseki J (1997) Inherent and stress system induced anisotropy in small strain stiffness of sandy gravel. Geotechnique 47(3):509–521 Thomas Telford Ed

Kaarsberg EA (1975) Elastic wave velocity measurement in rocks and other materials by phase-delay methods. Geophysics 40:901–955

Koseki J, Balakrishnaiyer K, Tatsuoka F (1999) Large scale triaxial tests on elastic properties of undisturbed gravel containing fines. Proceedings of the international symposium on pre-failure deformation characteristic of geomaterials. IS Torino, 1: 299–304

Lee Ch-J, Wang Ch-R, W-Yi Hung (2012) Evolution of the shear wave velocity during shaking modeled in centrifuge shaking table tests. Bull Earthq Eng 10(2):401–420

Lirer S, Flora A, Nicotera MV (2011) Some remarks on the coefficient of earth pressure at rest in compacted sandy gravel. Acta Geotecnica, 6(1): 1–12, Springer Ed. ISSN: 1861-1125

Mancuso C, Simonelli AL, Vinale F (1989) Numerical analysis of in situ S-wave measurement. Proceedings 12th International Conference on soil Mechanics, Rio de Janeiro, 3: 277–280

Marsal RJ (1967) Large scale testing of rockfill materials. J SMFE, ASCE 93(2):27–43

Mitatitonna G, Amorosi A, Cotecchia F (2010) Multidirectional bender element measurements in the triaxial cell: equipment set-up and signal interpretation. RIG Rivista Italiana di Geotecnica 44(1):50–69

Modoni G, Flora A, Mancuso C, Tatsuoka F, Viggiani C (2000) Evaluation of gravel stiffness by pulse wave transmission tests. ASTM Geotech Test J, GTJODJ 23(4):506–521

Robertson PK (1994). Suggested terminology for liquefaction. In Proceedings of the 47th Canadian geotechnical conference, Halifax, 277–286, N.S. CGS

Santamarina JC, Aloufi M (1999) Small strain stiffness: a micromechanical experimental study. Proceedings of the 2th international symposium on pre-failure deformation characteristic of geomaterials. IS Torino, 1: 451–458

Santamatina JC, Cascante G (1996) Stress anisotropy and wave propagation: a micromechanical view. Can Geotech J 33(5):770–782

Seed HB, Idriss IM, Arango I (1983) Evaluation of liquefaction potential using field performance data. J Geotech Eng, ASCE 109(3):458–482

Sharma SS, Fahey M (2004) Deformation characteristic of two cemented calcareous soils. Can Geotech J 41:1139–1151

Shirley DJ, Hampton LD (1978) Shear wave measurements in laboratory sediments. J Acoust Soc Am 63(2):607–613

Tanaka Y, Kokusho T, Yoshida Y, Kudo K (1991) A method for evaluating membrane compliance and system compliance in undrained cyclic shear tests. Soils Found 31(3):30–42

Tatsuoka F, Kohata Y (1994) Stiffness of hard soils and soft rocks in engineering applications. Proceedings of international symposium. On pre failure deformation of geomaterials, Rotterdam, Balkema, 947–1066

Tokimatsu K, Yoishida A (1990) Correlation between liquefaction resistance and shear wave velocity. Soils Found 30(2):33–42

Viggiani G, Atkinson JH (1995) Interpretation of bender element tests. Gèotechnique 45(1):149–154

Vinale F (1988) Caratterizzazione del sottosuolo di una area campione di Napoli ai fini della microzonazione sismica. Rivista Italiana di Geotecnica (RIG), 22 (2). In Italian

Youn J, Choo Y, Kim D (2008) Measurement of small strain shear modulus G_{max} of dry and saturated sands by bender elements, resonant column and torsional shear tests. Can Geotech J 45:1426–1438

Yunmin C, Han K, Ren-peng Ch (2005) Correlation of shear wave velocity with liquefaction resistance based on laboratory tests. Soil Dyn Earthq Eng 25(2005):461–469

Zhou JG, Chen YM (2007) Laboratory investigation on assessing liquefaction resistance of sandy soils by shear wave velocity. J Geotech Geoenviron Eng, ASCE, 959–972